Using Dispersion Analysis to Assess The Effective Resolution of Advection Schemes

James Kent[a,*], Jared P. Whitehead[a,b], Christiane Jablonowski[a], Richard B. Rood[a]

[a] *Department of Atmospheric, Oceanic and Space Science, University of Michigan, 2455 Hayward St., Ann Arbor, Michigan 48109-2143, USA*

[b] *Center for Nonlinear Studies, MS B258, Los Alamos National Laboratory, Los Alamos, New Mexico 87545, USA*

Abstract

The effective resolution of a numerical scheme describes the smallest spatial scale (largest wavenumber) that is completely resolved by that scheme. Investigating the dispersive and dissipative properties of a numerical scheme for the advection equation allows the effective resolution to be calculated. The advection equation is a fundamental building block of dynamical cores of atmospheric and ocean models, and this analysis provides an indication of the effective resolution of the numerical methods used by dynamical cores. Using a variety of finite-difference schemes, the effect on effective resolution of using explicit diffusion and hyper-diffusion terms is examined. The choice of order-of-accuracy, and the time-stepping of the numerical scheme is also investigated with regards to effective resolution. Finally, we apply this analysis to methods that are commonly used in dynamical cores of atmospheric general circulation models, namely semi-Lagrangian and finite-volume methods.

Keywords: Effective Resolution, Finite-Difference Methods, Finite-Volume Methods, Dispersion Analysis, Dynamical Core

1. Introduction

Atmospheric models are composed of a dynamical core which is coupled to a subgrid-scale parameterization package. The dynamical core is the fluid dynamics component of an atmospheric model, and it solves the adiabatic governing equations (usually the primitive equations under certain approximations, for example hydrostatic balance) and the equations governing the transport of tracers. Dynamical cores of weather and climate models make use of numerical methods to solve the equations governing fluid flow. There are many different types of numerical methods that are used in dynamical cores of general circulation models

*Corresponding author. Address: Department of Atmospheric, Oceanic and Space Science, University of Michigan, 2455 Hayward St., Ann Arbor, Michigan 48109-2143, USA. Tel.: + 1 734 763 6241.

Email addresses: jdkent@umich.edu (James Kent), whitehead@lanl.gov (Jared P. Whitehead), cjablono@umich.edu (Christiane Jablonowski), rbrood@umich.edu (Richard B. Rood)

(GCMs), such as finite-difference [10], finite-volume [25, 42], semi-Lagrangian [6, 51], spectral transform [11, 12], and spectral element [7]. It is important to understand the properties of different numerical methods, either to better understand the properties of an existing dynamical core, or to make an informed modeling choice when designing future models.

One property of a numerical method is the effective resolution. Whereas 'resolution' usually refers to the model's grid spacing, the effective resolution of a numerical scheme is generally defined as the smallest spatial scale (i.e. the largest wavenumber) that is 'fully resolved' by said numerical scheme. The shortest fully resolved wavelength, i.e. the effective resolution, is usually considerably larger than the grid spacing [45]. It is desirable to determine the effective resolution of a numerical scheme, and therefore the effective resolution of a model that makes use of the scheme. For example, in atmospheric modeling there is a desire to resolve features that are unresolved or only marginally resolved by current models, and thus improve weather forecasts and climate predictions [36]. As a higher effective resolution means that more features will be resolved by the model, increasing a model's effective resolution (through the choice of numerical methods) could prove a cheaper alternative to resolving small features than just doubling the grid resolution. This idea is closely related to the concept of 'equivalent resolution' as discussed in [50]. [50] determined the necessary grid spacings for two dynamical cores that led to equivalent simulation results when coupled to an identical physical parameterization package. He showed that similar results were obtained when the grid spacing in a finite-volume dynamical core was smaller than the Gaussian grid spacing in a spectral-transform dynamical core (e.g. 1° verse 1.4°). It suggests that the higher diffusion of the finite-volume method necessitates a finer grid spacing to match the 'effective resolution' of the less diffusive spectral method.

In addition, understanding the effects of explicit diffusion and filters on effective resolution provides insight into the tuning of diffusion coefficients (and the consequences of badly tuned parameters). With full GCMs the coupling of the subgrid-scale physical parameterization package and the "resolved" dynamical core is an important issue [8], and the physics parameterizations are often coupled to the dynamics at the grid scale. However, the dynamics do not truly resolve the grid scale, and it may be beneficial to add some of the physics to only the resolved scales i.e. the effective resolution [21]. Such GCM experiments with finer grid spacings in the dynamical core and coarser grids for the physics forcings were evaluated by [48]. For weather and climate models, composed of both dynamics and physics, [36] suggested numerically calculating the effective resolution based upon the departure of the kinetic energy spectra from a given power law. However, to calculate the effective resolution of numerical schemes that could be used in dynamical cores, analytical methods can be used, as proposed in this paper.

One tool to evaluate the properties of numerical schemes is dispersion analysis [33]. Linear dispersion analysis of numerical schemes for atmospheric models has previously been performed for a variety of methods [27, 31, 22, 37]. This dispersion analysis can be used to investigate dispersive properties (such as group velocity and phase speed) and diffusive properties, and can be used to determine accuracy and stability of the numerical scheme [40, 46]. Using dispersion analysis to measure the effective resolution of a numerical method was introduced by [44]. In [44], several different types of numerical methods (finite-volume,

spectral element, spectral finite-volume, and discontinuous Galerkin) were analyzed for the linear wave equation with exact time integration, and their dispersive and diffusive properties were used to determine the effective resolution for different orders of accuracy. The aim of our paper is to modify this analysis for use with different time integration methods, to show the impact of the time integration scheme and the choice of timestep on the effective resolution of advection schemes. We also investigate the effect of explicit diffusion and hyper-diffusion terms on the diffusive and dispersive properties of a numerical scheme, and therefore the effect this diffusion has on effective resolution. We investigate these issues using simple finite-difference schemes, before applying the analysis to semi-Lagrangian and finite-volume methods.

Some form of diffusion (either implicit in the numerics, as an explicitly added term, or in the form of a filter) is usually required for models solving non-linear governing equations on a fixed grid. There are a number of numerical reasons that a modeler might chose to add diffusion to their scheme, for example to improve stability, to damp computational modes, or to ensure monotonicity. For the constant velocity linear advection equation there is no physical reason for diffusion. However, for the non-linear governing equations there is the physical need for diffusion to correctly model transfers of quantities between resolved and unresolved scales. In numerical studies of three-dimensional turbulence (large eddy simulation - LES) a subgrid model is required to dissipate kinetic energy, as this represents the effects of the unresolved flow on the resolved flow [29]. For two-dimensional flow it is the enstrophy which cascades downscale to unresolved scales, and therefore must be dissipated [18]. The atmosphere is strongly multiscale, with many interactions between these scales. Due to the effects of stratification and rotation, the atmosphere may resemble two-dimensional flow at large scales [1], before transitioning to three-dimensional flow at smaller scales. In dynamical cores of atmospheric models the diffusion is used to prevent the accumulation of potential enstrophy and kinetic energy at the grid scale, and also to dissipate tracer variance in the transport scheme [38, 19]. This diffusion is often added in an ad-hoc way, and heavily tuned to provide optimal results [17]. This means that although diffusion is undesired in the linear dispersion analysis for the linear advection equation, it is an essential part of the numerical methods that make up the dynamical cores.

The linear analysis is performed on finite-difference schemes for the one-dimensional linear advection equation. The advection equation is an informative example to consider - many numerical schemes that are used for the advection equation can also be used to solve conservation laws, such as the continuity equation for fluid density or the vorticity equation for example. The multi-dimensional advection equation with non-constant velocities describes the transport of tracers in the atmosphere (without sources or sinks). Replacing the advected quantity with potential vorticity gives the equation for potential vorticity evolution, whereas replacing it with potential temperature gives the equation for potential temperature (in the absence of heating). The advection equation, and non-linear variations, appears in any equation that makes use of the material derivative, such as the momentum equations for the shallow water and primitive equation sets. It is thereby a fundamental building block of a dynamical core. The assessment of the effective resolution of the advection equation is thereby an informative predictor for the effective resolution of the non-linear dynamics

component. There are many different types of advection schemes (see, for example, [35]), of which we consider only a subset in this study.

This paper is structured as follows. Section 2 describes the one-dimensional linear advection equation that will be used for the analysis. Section 3 describes the dispersion analysis methodology. Using the dispersion analysis to determine the effective resolution of a number of numerical schemes is presented in section 4, where we use finite-difference schemes to show the effects of order-of-accuracy, diffusion and time-stepping on effective resolution. We then turn our attention to numerical methods that are commonly used in dynamical cores, such as semi-Lagrangian and finite-volume methods. Conclusions are drawn in section 5. Appendix A describes the dispersion analysis in detail, while Appendix B discusses the threshold used in our metrics to define effective resolution.

2. The Advection Equation

The one-dimensional advection equation is given as

$$\frac{\partial q}{\partial t} + u\frac{\partial q}{\partial x} = 0, \tag{1}$$

where $q(x,t)$ is a tracer mixing ratio, u is the constant velocity, and t is time. Note that all quantities are dimensionless in this paper, and that throughout we use $u = 1$. Since u is constant, the one-dimensional linear advection equation can also be written in flux form as

$$\frac{\partial q}{\partial t} + \frac{\partial uq}{\partial x} = 0. \tag{2}$$

The advective form (1) and the flux form (2) are interchangeable for constant velocities. The advection equation supports wavelike solutions of the form

$$q = \hat{q}\exp(i(kx - \omega t)), \tag{3}$$

where k is the spatial wavenumber, ω the frequency, $\hat{q}$ is the amplitude, and $i = \sqrt{-1}$ is the imaginary unit. The wavelike solutions allow the calculation of the dispersion relation

$$\omega = \omega(k), \tag{4}$$

and the amplitude factor

$$|\Gamma| = |\exp(-i\omega t)|. \tag{5}$$

Inserting the wavelike solutions into the advection equation (1) gives the analytical dispersion relation for advection as

$$\omega = uk, \tag{6}$$

and the analytical amplitude factor as

$$|\Gamma| = 1. \tag{7}$$

For numerical solutions to the advection equation an important quantity is the Courant number $c = u\Delta t/\Delta x$, where Δt is the timestep and Δx is the grid spacing. The Courant number is linked to the stability of a numerical scheme (it is common for methods to be unstable for $c > 1$). In fluid dynamics problems the velocity u is rarely constant, and therefore in this paper we consider the analysis over a number of Courant numbers. In this paper we only consider the case of uniform grid spacing, i.e. constant Δx.

3. Analysis of Advection Schemes

The methodology for calculating the amplitude factor and dispersion relation of a given numerical scheme is given in detail in Appendix A. We start by inserting the solution for the discrete tracer

$$q_j^n = \hat{q} \exp\left(i(kx_j - \omega t_n)\right), \tag{8}$$

into the scheme's discretization. Here j and n are the spatial and temporal indices, with $\Delta x = x_{j+1} - x_j$ and $\Delta t = t_{n+1} - t_n$. We divide each term in the discretization by (8), to give a relationship between the numerical amplitude factor $|\Gamma_{num}| = |\exp(-i\omega\Delta t)|$ and k. Here the subscript num indicates the amplitude factor for a numerical scheme over one time-step. The amplitude factor $|\Gamma|$ shows which wavenumbers k are damped or amplified by the numerical scheme. For the advection equation there should be no damping or amplification of any wavenumbers, and therefore $|\Gamma| = 1$. If the amplitude factor exceeds 1 for any k, then the scheme is unstable.

For a two time-level scheme, the resulting expression for the scheme's discretization will only contain the amplitude factor to the power one. For a three time-level scheme we obtain an expression which is quadratic in Γ, and thus requires the solution to the quadratic equation to give the amplitude factor in terms of k. Similarly, a four time-level scheme gives a cubic equation. Note that the correct root must be selected to give the actual amplitude factor of the physical mode, and not that of the computational mode.

We proceed by first calculating the amplitude factor and then the dispersion relation. The dispersion relation is a relationship between the frequency ω and the spatial wavenumber k. It can also be used to calculate the phase speed and the group velocity. Comparing a numerical scheme's dispersion relation with the true dispersion relation shows which wavenumbers are properly capturing the dispersive properties of the advection equation. The numerical dispersion relation can now be computed via (5) as

$$\omega = -\frac{\log \Gamma_{num}}{i\ \Delta t}. \tag{9}$$

We are interested in comparing the effect of choosing various timesteps for a given spatial grid. In order to provide a fair comparison, we evaluate the cumulative effect of the schemes to a final time T. This is equivalent to saying that for a Courant number of $c = 0.1$ the analysis must be repeated 10 times to give the corresponding result for analysis performed with $c = 1$. To make the analysis consistent, unless noted otherwise, we run to $c = 1$. Therefore, we set the number of timesteps as $m = 1/c$ and calculate the amplitude factor as

$$|\Gamma| = |\Gamma^m_{num}|, \tag{10}$$

and the dispersion relation as

$$\omega = -\frac{\log \Gamma^m_{num}}{i\ \Delta t\ m}. \tag{11}$$

3.1. Forward-in-Time Lax-Wendroff Type Schemes

Much of the analysis in this paper will feature the Lax-Wendroff advection scheme [24], and higher-order versions of it [39]. The Lax-Wendroff scheme is a second-order (in both space and time) scheme that solves the advection equation as

$$q^{n+1}_j = q^n_j - c\left(\tilde{q}^{n+\frac{1}{2}}_{j+\frac{1}{2}} - \tilde{q}^{n+\frac{1}{2}}_{j-\frac{1}{2}}\right), \tag{12}$$

with the *flux like* terms $\tilde{q}^{n+\frac{1}{2}}_{j-\frac{1}{2}}$ calculated as

$$\tilde{q}^{n+\frac{1}{2}}_{j-\frac{1}{2}} = \frac{1}{2}\left(q^n_j + q^n_{j-1}\right) - \frac{1}{2}c\left(q^n_j - q^n_{j-1}\right). \tag{13}$$

Here the half spatial indices relate to the midpoint between finite-difference points (or the cell edges of finite-volume cells). It is evident that the Lax-Wendroff scheme can be written in flux form (2), with the numerical fluxes given by $u\tilde{q}^{n+\frac{1}{2}}_{j\pm\frac{1}{2}}$. Increasing the order of the fluxes will increase both the temporal and spatial order of the scheme. Orders one to six are given in [39]. Note that the first-order scheme is just the first order upwind scheme. To leading order error, the odd ordered schemes are diffusive and the even order schemes are dispersive (although to higher order error the even order schemes contain diffusion terms). Calculating the amplitude factors of the Lax-Wendroff schemes shows that the odd ordered schemes damp more wavenumbers and to a larger magnitude than the even ordered schemes.

Diffusion and hyper-diffusion can be easily applied to the Lax-Wendroff type schemes. When additional hyper-diffusion terms of order $2p$ are used, the advection equation becomes the advection-diffusion equation of the form

$$\frac{\partial q}{\partial t} + u\frac{\partial q}{\partial x} = (-1)^{p+1}\mu_p \frac{\partial^{2p} q}{\partial x^{2p}}, \tag{14}$$

for $p = 1, 2, 3, 4...$, where μ_p is the diffusion coefficient. The diffusion coefficient is chosen as $\mu_p = \nu_p \Delta x^{2p}/\Delta t$, where ν_p is a constant. For the analysis in this paper we approximate second-order diffusion as

$$\frac{\partial^2 q}{\partial x^2} \approx \frac{1}{\Delta x^2}\left(q^n_{j+1} - 2q^n_j + q^n_{j-1}\right). \tag{15}$$

Higher-order hyper-diffusion can be generated by applying the diffusion approximation repeatedly (and switching the sign of the diffusion coefficient). A stronger diffusion coefficient for the diffusion terms results in stronger damping of the wavenumbers. Calculating the

amplitude factors of the hyper-diffusion (with exact time integration) shows the scale selective nature of high-order hyper diffusion; for example, when using diffusion coefficients such that the amplitude factor equals 0.8 at the $2\Delta x$ wave (i.e. where the dimensionless wavenumber $k\Delta x = \pi$), the second-order diffusion damps the $16\Delta x$ wave to the same extent as the eighth-order hyper-diffusion damps the $4\Delta x$ wave.

4. Determining Effective Resolution

Following [15, 44] we define a wavenumber k as being 'fully resolved' by a numerical scheme if the numerical scheme satisfies both the dispersive and diffusive properties of the advection equation at that wavenumber. To recap, for the linear advection equation the true dispersion relation is $\omega = uk$, and the true amplitude factor is $|\Gamma| = 1$. The numerical dispersion relation ω_N is classed as satisfied at wavenumber k if

$$\frac{|Re(\omega) - Re(\omega_N)|}{|Re(\omega)|} \leq \epsilon, \tag{16}$$

for wavenumber k at some error threshold ϵ. Similarly, the diffusive property is satisfied using the numerical amplitude factor Γ_N at wavenumber k if

$$\frac{||\Gamma| - |\Gamma_N||}{|\Gamma|} \leq \epsilon, \tag{17}$$

for wavenumber k. The effective resolution of a numerical scheme is thus defined as the shortest wave (with wavelength $N\Delta x$) which satisfies both the dispersion relation (16) and the diffusive property (17) metrics, for all waves with wavelength $\lambda \geq N\Delta x$. Therefore, a scheme has a better effective resolution and can resolve smaller scales for smaller values of N. Note again that in these calculations we take the cumulative amplitude factors and dispersion relations, (10) and (11), as we perform the analysis to a final time T (i.e. $m = 1/c$). In the following subsections, the plots of effective resolution against Courant number show the effective resolution when just the diffusive component is considered (i.e. metric (17)), the effective resolution when just the dispersive component is considered (i.e. metric (16)), and finally the effective resolution when both metrics are taken into account. Note that in the plots the lines stop at the Courant number the scheme becomes unstable, i.e. $|\Gamma| > 1$ for c to the nearest 0.05.

The choice of the threshold ϵ has a large impact on which wavenumbers are classified as resolved. This is discussed in detail in Appendix B. Following [44] we choose $\epsilon = 0.01$, i.e. the numerical dispersion relation and amplitude factor must be within 99% of the analytic value. Note that we are weighting the diffusive and dispersive errors equally. It would be viable to use different ϵ for diffusion and dispersion errors when calculating the effective resolution.

We use this methodology to investigate the effective resolution of finite-difference advection schemes. We use finite-difference schemes as a general case to highlight the effects of three modelling choices: order of accuracy; explicit diffusion; and time-stepping. We

then focus on numerical methods that are relevant to dynamical cores, investigating semi-Lagrangian schemes (section 4.4) and finite-volume schemes (section 4.5).

4.1. Order of Accuracy

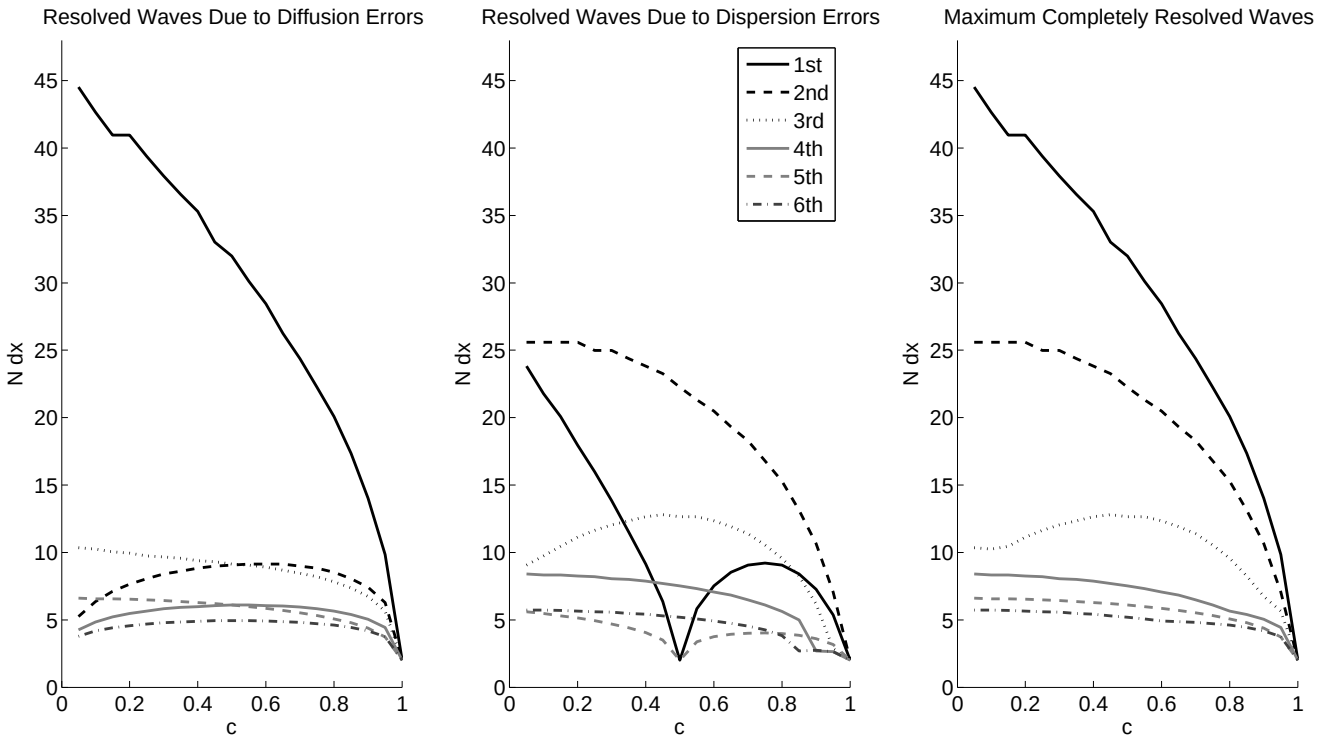

Figure 1: The maximum resolved wave (in terms of $N\Delta x$) for $\epsilon = 0.01$ due to diffusion errors (left), dispersion errors (center), and both diffusion and dispersion error (right), for Lax-Wendroff schemes of order 1 to 6.

In general, for smooth data, a numerical method with a higher formal order of accuracy will be more accurate than a scheme with a lower order of accuracy. However, increasing the order of accuracy of a numerical scheme is usually computationally expensive, especially for multi-dimensional schemes. Hence there is a need to consider the effect of increased accuracy with increased cost [20]. In this section we show the effects of increased accuracy on effective resolution.

We use the Lax-Wendroff method [24] to investigate the effect of the order of accuracy of a numerical scheme on the effective resolution. The second-order Lax-Wendroff scheme can be extended up to arbitrary order of accuracy [39]. Here we use orders $2-6$, and also include the first-order upwind scheme.

Figure 1 shows the maximum resolved wave (in terms of $N\Delta x$) for $\epsilon = 0.01$ for the Lax-Wendroff type schemes for Courant numbers $0 < c \leq 1$. The effective resolution when only the diffusive component is considered is shown in the left plot. The effective resolution when only the dispersive component is considered is shown in the center plot. The right plot shows

the effective resolution when both the diffusive and dispersive components are considered, and therefore is the maximum of the left and center plot for each Courant number. Note that the first-order scheme has zero dispersion errors at $c = 0.5$. The dispersion relation for the first-order scheme curves away below the true dispersion relation for $0 < c < 0.5$ and above the true dispersion relation for $0.5 < c < 1$. Using modified equation analysis (see [14] or [28] for example) to calculate the truncation error of the first-order scheme, up to order $O(\Delta x^2)$, gives

$$\begin{aligned}\frac{\partial q}{\partial t} + u\frac{\partial q}{\partial x} =& \frac{u\Delta x}{2!}(1-c)\frac{\partial^2 q}{\partial x^2} \\ &+ \left[\frac{u^2\Delta t\Delta x}{2!}(1-c) - \frac{u\Delta x^2}{3!}\left(1-c^2\right)\right]\frac{\partial^3 q}{\partial x^3} + H.O.T. \end{aligned} \tag{18}$$

The leading order error is the diffusive $\partial^2 q/\partial x^2$ term, and the leading dispersion error is the $\partial^3 q/\partial x^3$ term. For $0 < c < 0.5$ the dispersion error term is negative, whereas for $0.5 < c < 1$ this term is positive, hence the switch in dispersion relation. At $c = 0.5$ the dispersion error term equals zero. This is also true for the fifth-order scheme. Note also that at $c = 1$ both the diffusive and dispersive error terms become zero, meaning that the first-order scheme has zero error for $c = 1$. This is also true for the higher-order Lax-Wendroff schemes, hence the effective resolution reverts to $2\Delta x$ at $c = 1$, because each of these schemes has zero error for a Courant number of unity.

As seen in the right plot of Figure 1, the increase in order of accuracy results in a higher effective resolution for the Lax-Wendroff schemes, as expected. However, the level of improvement decreases as the order of accuracy gets higher. For example, the increase in effective resolution from first to second-order is approximately $20\Delta x$ for $c = 0.05$, and the increase from fourth to fifth-order is approximately $2\Delta x$ for $c = 0.05$.

These results can also show us the effectiveness of increasing the grid resolution. For example, for $c = 0.05$ the second-order Lax-Wendroff scheme has an effective resolution of approximately $26\Delta x$. Doubling the grid resolution would result in the second-order Lax-Wendroff scheme resolving $26\Delta x$ of the fine grid, and $13\Delta x$ of the original, coarse grid. However, the third-order Lax-Wendroff scheme resolves approximately $10\Delta x$ on the original, coarse grid. This implies that it is beneficial (in terms of number of resolved waves) to use the third-order Lax-Wendroff scheme on the coarse grid rather than the second-order Lax-Wendroff scheme on the finer grid.

4.2. Effect of Explicit Diffusion

Explicit diffusion terms can be applied to the Lax-Wendroff schemes used in the previous section. The coefficients in this section are chosen to illustrate the effects of diffusion on effective resolution.

The use of second-order diffusion with the second-order Lax-Wendroff scheme is shown in Figure 2. Three diffusion coefficients are used, each increasing in magnitude by a factor of two. The use of explicit diffusion increases the diffusion errors of the scheme, but it can

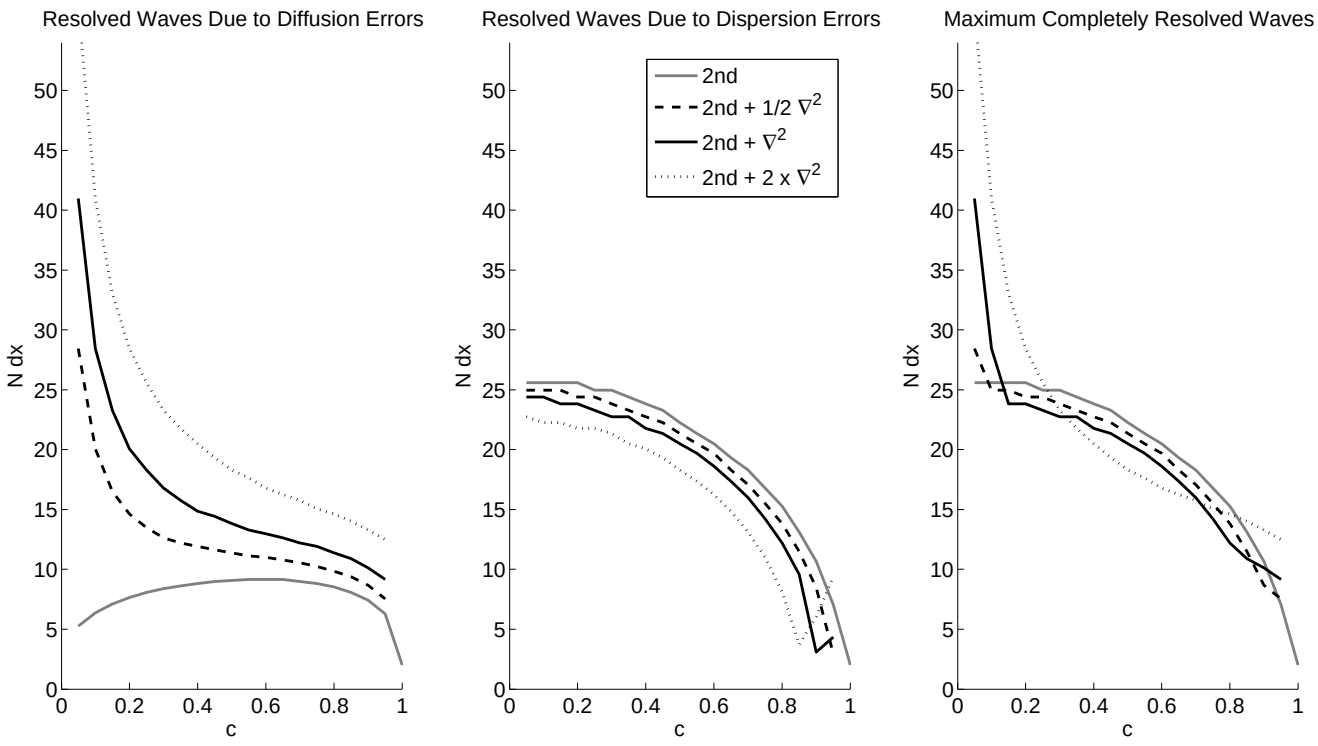

Figure 2: The maximum resolved wave (in terms of $N\Delta x$) for $\epsilon = 0.01$ due to diffusion errors (left), dispersion errors (center), and both diffusion and dispersion error (right), for the second-order Lax-Wendroff scheme with ∇^2 diffusion of different coefficient strength.

also remedy some of the dispersion errors in the second-order Lax-Wendroff scheme. The choice of diffusion coefficient becomes important, as it is desirable to decrease dispersion errors without producing too many diffusion errors. Using explicit diffusion and the 'right' coefficient with the second-order Lax-Wendroff scheme can improve the effective resolution of the scheme. At $c = 1$, the second-order scheme with no diffusion has zero dispersive error, and therefore can resolve the $2\Delta x$ wave based on the dispersion metric (this is shown in the center plot of Figure 2). In general though, adding the diffusion terms reduces the dispersion error, and therefore the schemes with the diffusion and hyper-diffusion achieve (nearly) zero dispersive error at Courant numbers less than 1. Then as $c \to 1$, the additional diffusion terms do not cancel the dispersion errors, and the resolved waves due to dispersion errors increase for each of the schemes with diffusion. The schemes with explicit diffusion and hyper-diffusion terms become unstable at $c = 1$.

We also consider the effects of higher-order hyper-diffusion by applying different ordered hyper-diffusion with the fourth-order Lax-Wendroff scheme (not shown). The diffusion coefficients are chosen such that each hyper-diffusion will damp the amplitude factor to the same level (i.e. $|\Gamma| = 0.8$ at $k\Delta x = \pi$). As with the second-order diffusion, the hyper-diffusion increases diffusion errors, but decreases dispersion errors. The lower ordered hyper-diffusion,

fourth- and sixth-order, has the most effect on the diffusion and dispersion errors, with higher-order hyper-diffusion (eighth-order and above, i.e. $p \geq 4$ in (14)) having almost no effect on the effective resolution of the fourth-order scheme.

4.3. Time-stepping Scheme

Section 4.1 shows the effective resolution when forward-in-time, Lax-Wendroff type time-stepping is used. Here we show the effective resolution for second and fourth-order spatial schemes with different types of time-stepping. We consider leapfrog, Adams-Bashforth [9], Runge-Kutta [13], and implicit Euler and implicit time-centered time-stepping schemes.

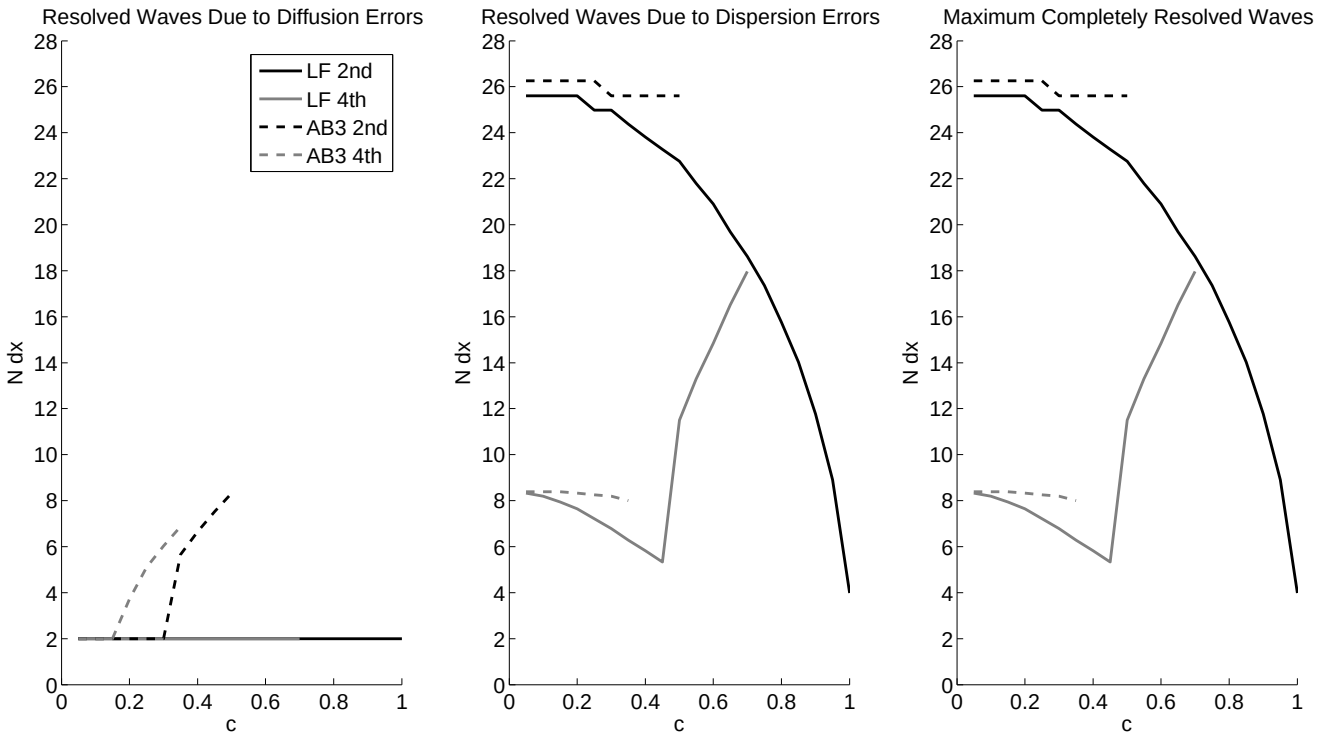

Figure 3: The maximum resolved wave (in terms of $N\Delta x$) for $\epsilon = 0.01$ due to diffusion errors (left), dispersion errors (center), and both diffusion and dispersion error (right), for leapfrog (LF) and third-order Adams-Bashforth (AB3) schemes with spatial order 2 and 4. The lines end stability limit of the schemes, i.e. at the last stable Courant number.

The leapfrog scheme is temporally second order, and discretizes the advection equation as a centered difference approximation in time

$$q_j^{n+1} = q_j^{n-1} - 2u\Delta t \frac{\partial q_j}{\partial x}. \tag{19}$$

Leapfrog time-stepping is common with both spectral and finite difference methods (such as the vertical discretization of [10]). In this paper, the spatial derivative is approximated using the second order approximation

$$\frac{\partial q_j}{\partial x} \approx \frac{1}{2\Delta x}\left(q^n_{j+1} - q^n_{j-1}\right), \tag{20}$$

and the fourth-order approximation

$$\frac{\partial q_j}{\partial x} \approx \frac{1}{12\Delta x}\left(-q^n_{j+2} + 8q^n_{j+1} - 8q^n_{j-1} + q^n_{j-2}\right). \tag{21}$$

The third-order Adams-Bashforth method [9] makes use of data at four-time levels, and is discretized as

$$q^{n+1}_j = q^n_j - u\frac{\Delta t}{12}\left(23\frac{\partial q^n_j}{\partial x} - 16\frac{\partial q^{n-1}_j}{\partial x} + 5\frac{\partial q^{n-2}_j}{\partial x}\right). \tag{22}$$

Figure 3 shows the effective resolution for second and fourth-order spatial schemes when using leapfrog and Adams-Bashforth time-stepping. The Adams-Bashforth method is temporally third-order. As leapfrog and Adams-Bashforth time-stepping make use of three and four time-levels respectively, in the calculation of $|\Gamma|$, a quadratic equation must be solved for the leapfrog schemes, and a cubic for the Adams-Bashforth schemes. The two roots of the quadratic equation for Γ (or the three roots of the cubic equation) correspond to the physical and computational modes. The physical mode is chosen for the results in this paper.

The plots end at the Courant number that the schemes become unstable, and this shows the stability limits of the fourth-order leapfrog scheme and of the Adams-Bashforth schemes for advection.

The effective resolution for the spatially second-order Adams-Bashforth scheme is around $25\Delta x$, and it is the dispersion errors that dominate this scheme. The fourth-order version has an effective resolution that is closer to the $9\Delta x$ wave. The second-order leapfrog scheme has zero diffusion error, but large dispersion errors for low Courant numbers. Similar to the Lax-Wendroff schemes, the effective resolution of the second-order leapfrog scheme improves as the Courant number approaches unity. The fourth-order version of the leapfrog scheme also has zero diffusion errors, although the stability criterion is exceeded at $c \approx 0.73$. However, the dispersion errors for the fourth-order leapfrog scheme increase with higher Courant numbers, showing how the second-order accuracy of the time-stepping becomes important near the stability limit.

The Robert-Asselin time filter [34, 2] is a method to damp the computational mode associated with the leapfrog scheme. It is commonly used for models that employ a three-time-level approach such as the Community Atmosphere Model Eulerian (CAM-EUL) pseudo spectral dynamical core [32]. It is an approximation of the second temporal derivative, and is discretized as

$$q^n_j = \kappa q^{n+1}_j - (2\kappa - 1)q^n_j + \kappa q^{n-1}_j, \tag{23}$$

where κ is the filter coefficient. The effective resolution for the spatially second-order leapfrog scheme with the application of the Robert-Asselin time filter is shown in Figure 4. We

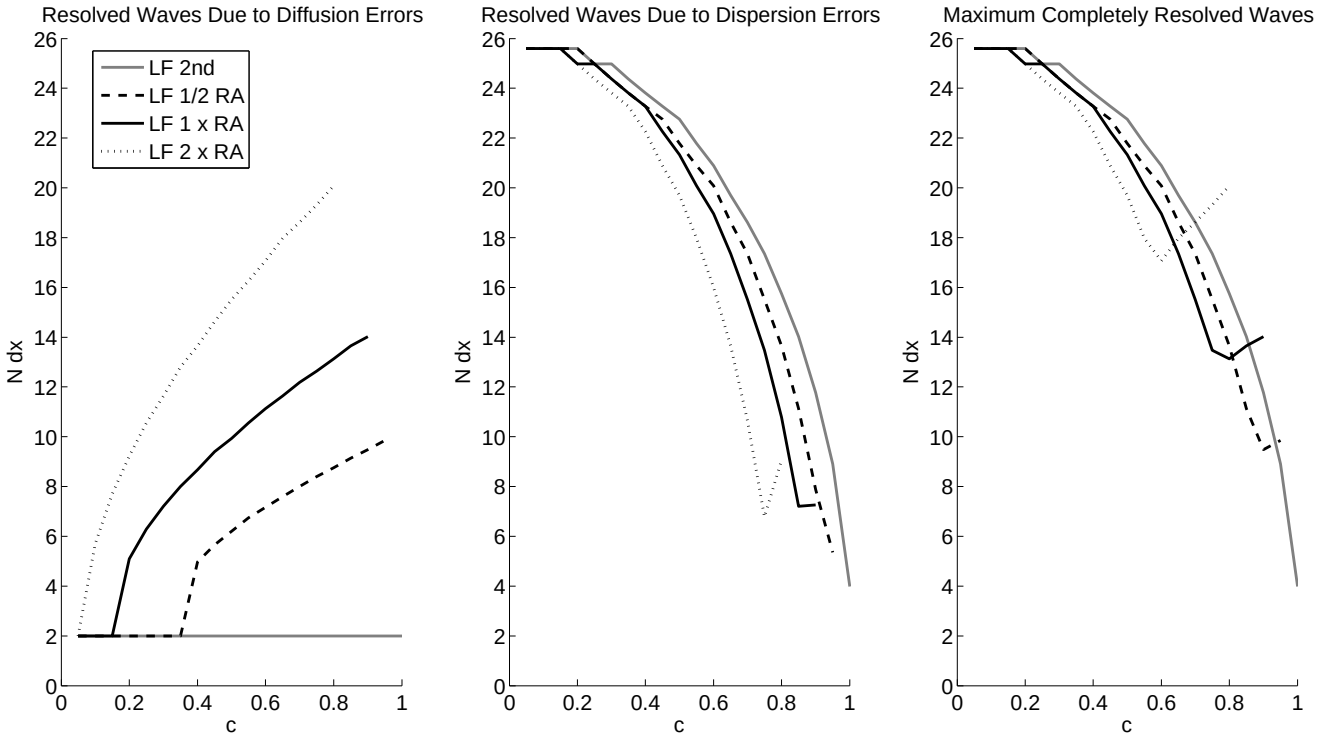

Figure 4: The maximum resolved wave (in terms of $N\Delta x$) for $\epsilon = 0.01$ due to diffusion errors (left), dispersion errors (center), and both diffusion and dispersion error (right), for the second-order leapfrog (LF) scheme with the application of different strength Robert-Asselin (RA) filter (0.05, 0.1 0.2).

consider the effect of different strength filter coefficients, $\kappa = 0.05$, 0.1 and 0.2. The effect of the time-filter is similar to the explicitly added spatial diffusion as seen in Figure 2: the time filter can reduce the dispersion errors and can produce a higher effective resolution than if no filter is used. Again, the schemes with the diffusion (in this case from the Robert-Asselin filter) have a minimum of dispersion errors at Courant numbers less than 1. Due to this, the diffusion errors rise for the schemes with the Robert-Asselin filter as $c \to 1$. The upturn in the effective resolution for the filtered schemes, shown in the right plot of Figure 4, is where the diffusion errors (from the Robert-Asselin filter) exceed the dispersion errors. The leapfrog schemes with different strength Robert-Asselin filters become unstable before $c = 1$, with the stronger coefficient resulting in a lower stability criteria.

The Runge-Kutta schemes are a family of time-stepping schemes that have been used in a variety of atmospheric problems [16, 41, 47]. Here we use the third and fourth-order versions. The third-order Runge-Kutta requires three steps, and is discretized as

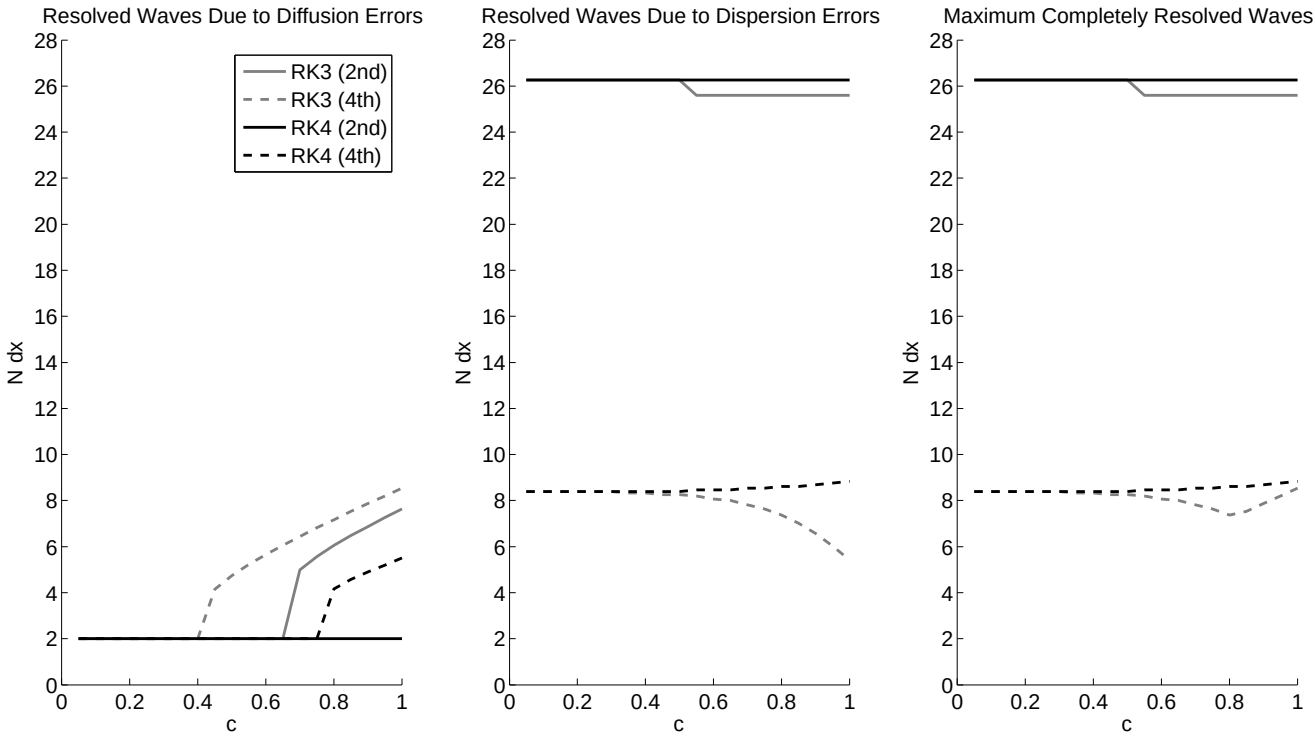

Figure 5: The maximum resolved wave (in terms of $N\Delta x$) for $\epsilon = 0.01$ due to diffusion errors (left), dispersion errors (center), and both diffusion and dispersion error (right), for third- and fourth-order Runge-Kutta (RK3 and RK4) schemes with spatial order 2 and 4.

$$q_j^* = q_j^n - u\frac{\Delta t}{3}\frac{\partial q_j^n}{\partial x}, \tag{24}$$

$$q_j^{**} = q_j^n - u\frac{\Delta t}{2}\frac{\partial q_j^*}{\partial x}, \tag{25}$$

$$q_j^{n+1} = q_j^n - u\Delta t\frac{\partial q_j^{**}}{\partial x}. \tag{26}$$

339 The fourth-order Runge-Kutta [13] is given as

$$k_1 = \frac{\partial q_j^n}{\partial x}, \tag{27}$$

$$k_2 = \frac{\partial (q_j^n - 0.5\ u\Delta t k_1)}{\partial x}, \tag{28}$$

$$k_3 = \frac{\partial (q_j^n - 0.5\ u\Delta t k_2)}{\partial x}, \tag{29}$$

$$k_4 = \frac{\partial (q_j^n - \ u\Delta t k_3)}{\partial x}, \tag{30}$$

$$q_j^{n+1} = q_j^n - u\frac{\Delta t}{6}\left(k_1 + 2k_2 + 2k_3 + k_4\right). \tag{31}$$

Figure 5 shows the effective resolution of second and fourth order spatial schemes when used with the third and fourth-order version of the Runge-Kutta method. The results are similar to the Adams-Bashforth methods shown in Figure 3, except that the Runge-Kutta methods are stable for all shown Courant numbers. The dispersion errors dominate the effective resolution for all the Runge-Kutta schemes tested. The spatial order appears to have a significant influence on the effective resolution; an increase in the spatial order from second to fourth produces a significantly better effective resolution for both Runga-Kutta methods. As the Runge-Kutta methods are temporally third and fourth-order, for the fourth-order spatial schemes there is not the sudden increase in the dispersion errors around $c \approx 0.4$ that can be seen for the spatially fourth-order and temporally second-order leapfrog scheme in Figure 3.

We now consider common implicit time-stepping schemes. Implicit time-stepping schemes are used because they are generally unconditionally stable, although they require the solution of an elliptic equation at each timestep. The implicit Euler method, which is only first-order in time, is discretized as

$$q_j^{n+1} = q_j^n - u\Delta t\frac{\partial q_j^{n+1}}{\partial x}. \tag{32}$$

The implicit time-centered scheme, which is temporally second-order, is discretized as

$$q_j^{n+1} = q_j^n - u\frac{\Delta t}{2}\left(\frac{\partial q_j^{n+1}}{\partial x} + \frac{\partial q_j^n}{\partial x}\right). \tag{33}$$

The effective resolution when the implicit Euler and implicit time-centered methods are used is shown in Figure 6. Here, second and fourth-order spatial schemes are used with the implicit Euler and implicit time centered methods. The implicit Euler method is only first-order accurate, hence the poorer effective resolution than the implicit time-centered scheme (for both spatial orders). The time-centered method produces zero diffusion errors, and therefore the maximum resolved wave due to diffusion is $2\Delta x$. Increasing the spatial order of accuracy from second to fourth-order improves the dispersion errors for both time integrations. As the Courant number increases, the effective resolution gets worse for all

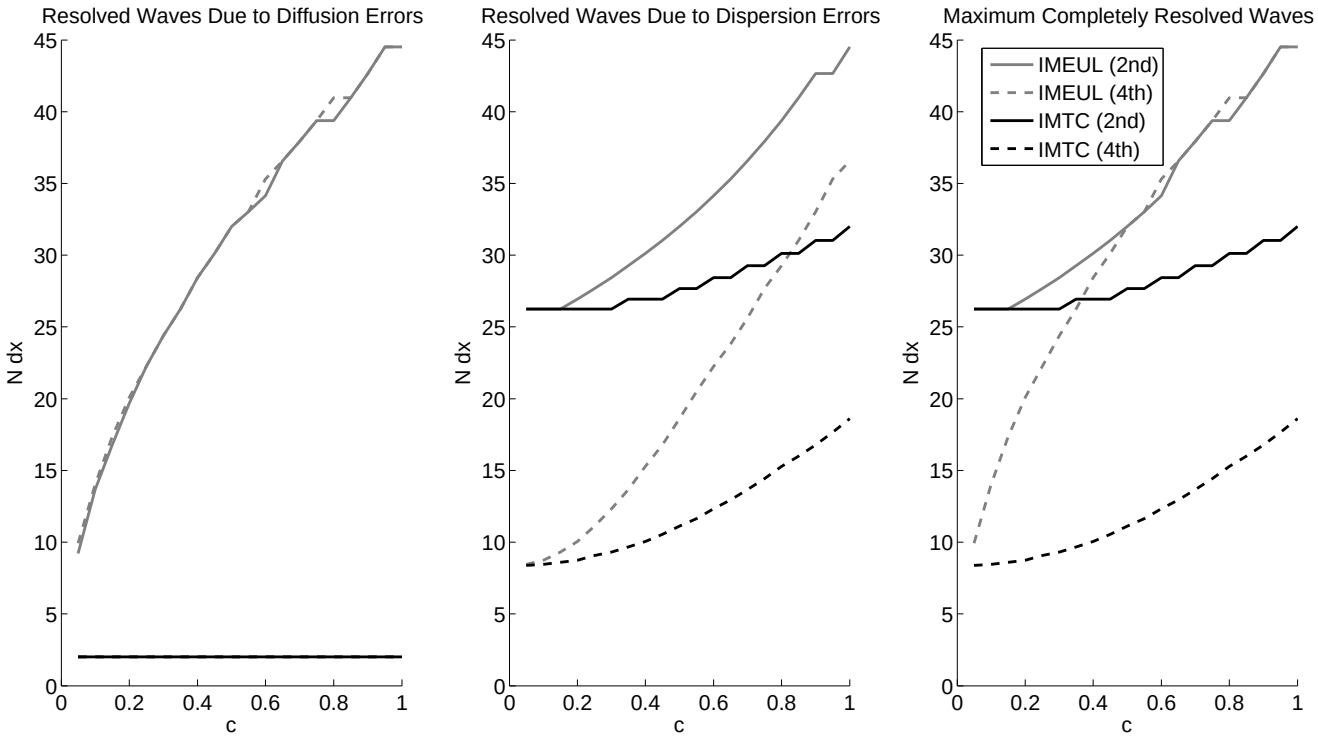

Figure 6: The maximum resolved wave (in terms of $N\Delta x$) for $\epsilon = 0.01$ due to diffusion errors (left), dispersion errors (center), and both diffusion and dispersion error (right), for implicit Euler (IMEUL) and implicit time-centered (IMTC) schemes, all with spatial order 2 and 4.

schemes. This is due to the accuracy of the time-stepping (first-order for implicit Euler, second-order for implicit time-centered) degrading with increased timestep Δt.

4.4. Semi-Lagrangian Schemes

Semi-Lagrangian schemes were historically used in dynamical cores that made use of latitude-longitude grids [49]. This was to reduce the impact of the convergence of the meridians at the pole, and allow larger timesteps to be taken. Semi-Lagrangian schemes are often used for transport in global spectral models, as it is easier to ensure positivity with semi-Lagrangian schemes than with spectral methods. Recent advances, such as conservative and high-order monotonic versions [23, 52, 43], indicates that semi-Lagrangian methods still have a part to play in the next generation of dynamical cores.

Here we use semi-Lagrangian schemes with no limiting. The semi-Lagrangian schemes can be written in finite-difference formulation, as given by [30]. For example, the semi-Lagrangian scheme with linear interpolation is given as

$$q_j^{n+1} = \alpha q^n_{j-(1+\mathrm{int}(c))} + (1-\alpha) q^n_{j-\mathrm{int}(c)}, \tag{34}$$

where $\alpha = c - \text{int}(c)$. The formula for quadratic, cubic and quartic interpolation is given by [30].

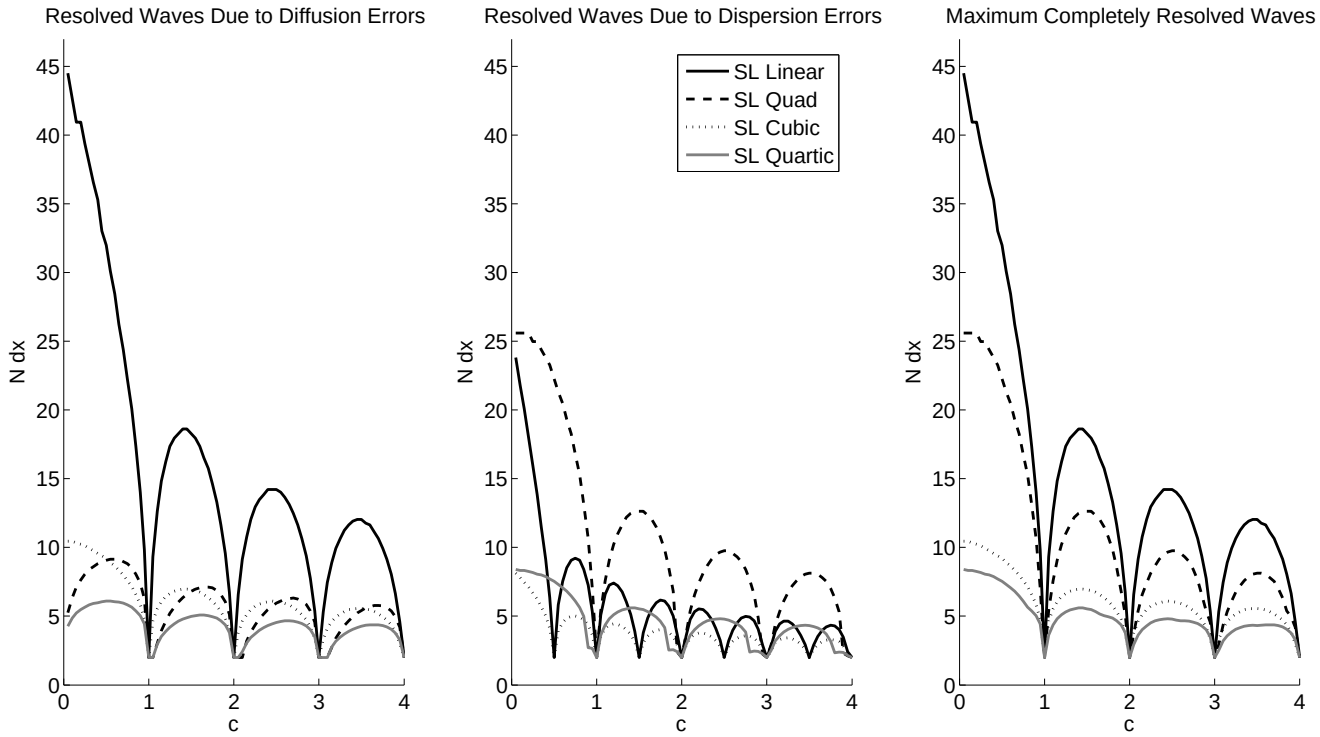

Figure 7: The maximum resolved wave (in terms of $N\Delta x$) for $\epsilon = 0.01$ due to diffusion errors (left), dispersion errors (center), and both diffusion and dispersion error (right), for two-time-level semi-Lagrangian (SL) schemes with linear, quadratic, cubic and quartic interpolation.

The effective resolution of semi-Lagrangian schemes using linear, quadratic, cubic and quartic interpolation is shown in Figure 7. One of the strengths of the semi-Lagrangian scheme is that it remains stable for long timesteps with $c > 1$. For this reason we show results up to Courant number $c = 4$, although to be consistent with the other schemes in this paper we assume that they are only simulated until $c = 1$, i.e. $m = 1/c$ in (10). The results for $c \leq 1$ are identical to those obtained using the Lax-Wendroff type schemes of order one to four, shown in Figure 1. For integer Courant numbers the advection is exact, and therefore all schemes are able to resolve the $2\Delta x$ wave. For each scheme, the pattern of diffusion and dispersion errors follows a similar quadratic curve between integer Courant numbers. The magnitude of this pattern decreases as the Courant number increases, because the simulation is only run to time $c = 1$.

The results for the semi-Lagrangian scheme with $c > 1$ are identical to those that can be obtained by running the Lax-Wendroff schemes (of order one to four) with a long time-step extension, such as the flux-form semi-Lagrangian approach of [26]. Note that these schemes are only equivalent for the linear constant velocity advection equation (1) that is considered

in our paper.

4.5. Finite-Volume Schemes

Finite-volume methods contain a number of desirable qualities (such as conservation, ease of applying limiters, and being a local method) and as such have been used in a number of dynamical cores of GCMs (for example [25, 42]).

The flux form equation (2) is numerically solved using fluxes F as

$$\frac{\partial q_j}{\partial t} = -\frac{\left(F_{j+\frac{1}{2}}^{n+\frac{1}{2}} - F_{j-\frac{1}{2}}^{n+\frac{1}{2}}\right)}{\Delta x}, \tag{35}$$

where the fluxes are calculated using subgrid distributions, $\tilde{q}$. The subgrid distributions make use of the cell volumes and cell edge reconstructions, $q_{j\pm\frac{1}{2}}$, and the type of distribution determines which finite-volume scheme is being used. For distributions that are discontinuous at the cell edges a Riemann flux operator is used. For the linear advection equation (with positive u) this becomes the upwind flux

$$F_{j+\frac{1}{2}} = u\tilde{q}_j\left(x_j + \frac{\Delta x}{2}\right). \tag{36}$$

For continuous distributions the flux is given as

$$F_{j+\frac{1}{2}} = uq_{j+\frac{1}{2}}. \tag{37}$$

Finite-volume methods have much in common with conservative finite-difference schemes (note that the forward-in-time Lax-Wendroff type schemes, section 3.1, calculate fluxes and can easily be applied to the conservative form of the equation), and as such some finite-volume methods are equivalent to some of the finite-difference schemes discussed in this paper. For example, the finite-volume method with piecewise constant subgrid distribution is just the first-order upwind scheme. The fourth-order centered edge reconstruction

$$q_{j+\frac{1}{2}} = \frac{-q_{j+2} + 7q_{j+1} + 7q_j - q_{j-1}}{12} + O(\Delta x^4) \tag{38}$$

becomes the fourth-order approximation of $\partial q/\partial x$ given by (21).

To investigate the effective resolution of finite-volume methods we use the second-order and third-order upwind schemes from [40], with both third-order and fourth-order Runge-Kutta time-stepping. We also use the unlimited piecewise parabolic method (PPM) of [4]. PPM uses the fourth-order edge reconstruction (38) to calculate $q_{j+\frac{1}{2}}$ and a third-order parabolic subgrid distribution, although we also show results for both the second and third-order edge reconstructions. Normally a limiting procedure is applied to make the reconstruction piecewise and discontinuous at cell edges, so that in each cell $qR_j = \tilde{q}_j\left(x_j + \frac{\Delta x}{2}\right)$ and $qL_j = \tilde{q}_j\left(x_j - \frac{\Delta x}{2}\right)$. Here, qL_j and qR_j are the left and right edge reconstructions of cell j. In the linear analysis applied in this paper no limiting is used, so that $qR_j = qL_{j+1} = q_{j+\frac{1}{2}}$. The flux is then calculated as

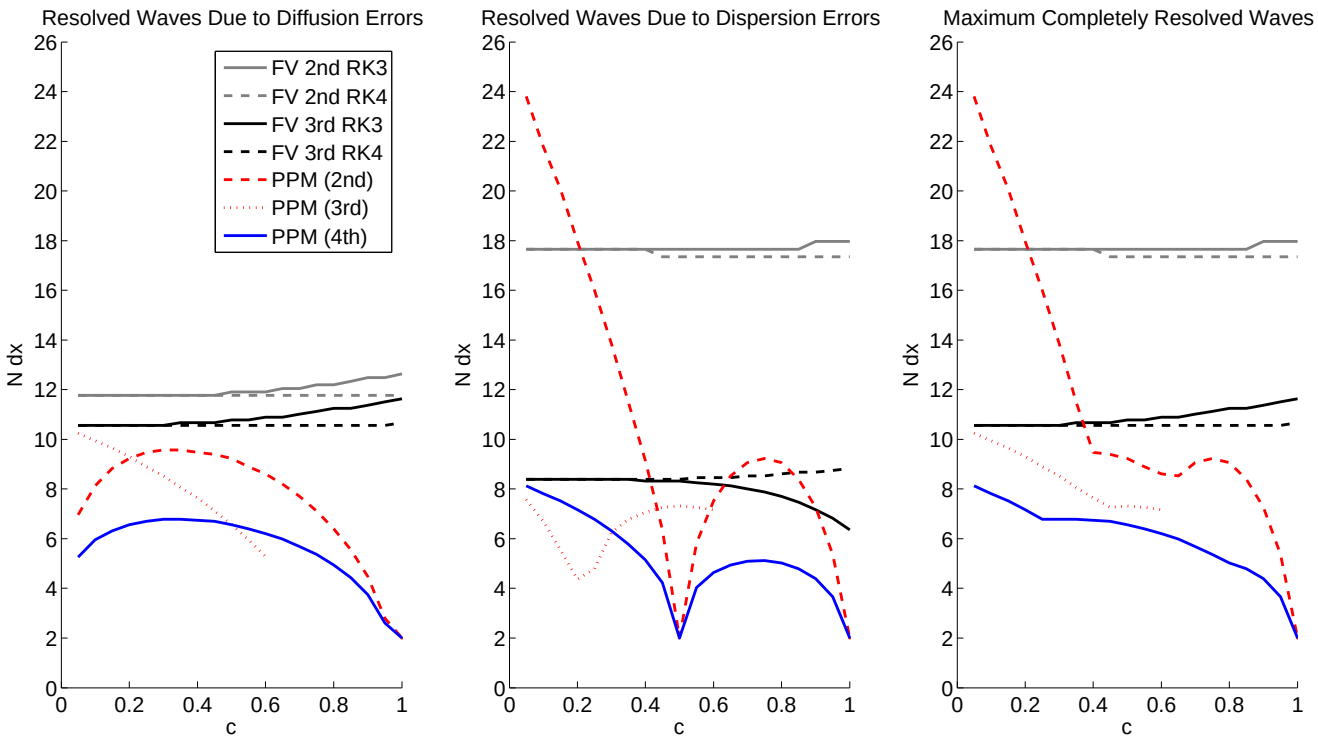

Figure 8: The maximum resolved wave (in terms of $N\Delta x$) for $\epsilon = 0.01$ due to diffusion errors (left), dispersion errors (center), and both diffusion and dispersion error (right), for the second-order upwind with Runge-Kutta 3 and Runge-Kutta 4 time-stepping, the third-order upwind with Runge-Kutta 3 and Runge-Kutta 4 time-stepping, and the piecewise parabolic method (PPM) with second, third and fourth-order edge reconstructions, finite-volume schemes.

$$F_{j+\frac{1}{2}} = qR_j - \frac{c}{2}\left(qR_j - qL_j - \left[1 - \frac{2c}{3}\right](6q_j - 3qL_j - 3qR_j)\right). \tag{39}$$

Figure 8 shows the effective resolution of the above mentioned finite-volume schemes for Courant numbers between 0 and 1. As with the finite-difference methods, the second-order scheme's effective resolution is dominated by dispersion errors, whereas the third-order scheme's effective resolution is dominated by diffusion errors. The third-order upwind scheme can resolve smaller scales than the second-order upwind scheme. The Runge-Kutta time-stepping for the finite-volume schemes produces simiar results to the Runge-Kutta time-stepping with finite-difference schemes (figure 5). For PPM, increasing the order of accuracy of the edge reconstruction improves the effective resolution, similar to the forward-in-time Lax-Wendroff type schemes. PPM with the third-order edge reconstruction becomes unstable for $c > 0.6$. PPM with the fourth-order edge reconstruction outperforms, in terms of effective resolution, all the other finite-volume methods tested here, for all $0 < c \leq 1$.

5. Discussion and Conclusions

The effective resolution of a numerical scheme is the smallest scale that is fully resolved by that numerical scheme. We have provided a method to analytically determine the effective resolution of numerical schemes for the linear advection equation using linear dispersion analysis. The dispersion analysis calculates the diffusive and dispersive errors at each wavenumber, and by defining an appropriate tolerance, we can determine if a wave is resolved or not based on these errors. In this study we use finite-difference schemes to investigate the role of the timestep in the dispersion analysis, and thus calculate the effective resolution across a range of Courant numbers. We also look at the role of explicit diffusion, in the form of hyper-diffusion and the Robert-Asselin filter, and how this contributes to the diffusion and dispersion errors. The analysis is then applied to schemes that are often used in dynamical cores of GCMs: semi-Lagrangian and finite-volume schemes.

The results show that increasing the spatial order of accuracy of the numerical scheme increases the scheme's effective resolution, regardless of the time-stepping scheme used. The sensitivity to the order of the time-stepping scheme is more complex and less predictable. As temporal order increases there is sensitivity to the Courant number with first-order discontinuities. The temporal sensitivity includes the onset of instability at smaller Courant numbers for the higher order schemes. For low-order temporal methods at large Courant numbers there is small sensitivity, and the spatial order of accuracy dominates the effective resolution. When increasing the spatial order of accuracy of a scheme by one, the greatest improvement is found for low order schemes (for example increasing from first to second-order, or from second to third-order), whereas the improvement diminishes for higher-order schemes. The results verify the conclusions of [20] that fourth-order accuracy appears to be 'optimal' in terms of improvement in accuracy relative to computational cost (note that [20] only considered spatial finite-differences). It can be shown that for some schemes increasing the order of accuracy is more beneficial, in terms of effective resolution, than just doubling the grid resolution. The same results are found with the semi-Lagrangian and finite-volume schemes - for example, at small Courant numbers the third and fourth-order edge reconstruction versions of the PPM algorithm fully resolve smaller scales than the second-order edge reconstruction PPM with doubled spatial resolution.

Explicit diffusion, hyper-diffusion, and the use of the Robert-Asselin filter increase the diffusion errors but can reduce the dispersion errors. This suggests that an optimal balance between diffusion and dispersion errors can increase the effective resolution of a scheme. This explicit diffusion is fundamentally non-physical as this analysis is applied to the advection equation at constant velocity, for which there is formally no diffusion. For advection in sheared flows and in dynamical cores of weather and climate models diffusion is required to model the downscale cascade of certain quantities. This is a difficult-to-quantify physical diffusion, which is in practice conflated with diffusion intrinsic to a numerical scheme and with diffusion that might be added to counter deficiencies in the discrete equations. The addition of physical diffusion also impacts the balance between diffusive and dispersive errors. These conflated roles of diffusion are a fundamental attribute of numerical advection schemes, and need to be considered not only in design but in analysis of the performance of

the model. The assumption that the impact of diffusion errors is small is often unjustified.

The effective resolution of a numerical scheme is an important point to consider when developing a dynamical core. For a GCM using $1^\circ \times 1^\circ$ resolution, the grid spacing at the equator is approximately 110 km. As shown for both finite-differences and finite-volumes, a second-order scheme may only fully resolve around $18 - 26\Delta x$ at low Courant numbers. This will correspond to the 1° GCM being unable to resolve fully features smaller than $\sim 2000 - 2800$ km. For models with variable resolution grids, it is possible for the numerical scheme to lose an order-of-accuracy at the change in resolution [10]. Therefore a second-order scheme on a variable resolution grid might revert to first-order at the resolution change, and, as shown in Figure 1, could find the effective resolution drop by $20\Delta x$, possibly negating the benefits of the variable resolution mesh.

Climate and weather models have a full complement of physics routines and realistic coupling between the surface and the atmosphere. Physics parameterizations, steep topographical features and shoreline boundaries often are on the grid scale [3]. The results in this paper show with clarity that in most cases a reasonable expectation is that the smallest fully resolved scale in the fluid dynamics is from 6 to 10 grid cells. Therefore, there is always a gap between the grid-scale physics and the dynamics. How to best manage errors and integrate information in this spatial range where the discretization errors are changing rapidly is not well understood.

It is not unusual to see the resolution of a model described as the size of the grid cell. To illustrate the importance of the role of effective resolution in a comprehensive model, consider the important impacts that the Great Lakes have on the weather and climate of surrounding land. The Great Lakes are not explicitly modeled in climate models. At the commonly used resolution of 1° latitude, the largest of the Great Lakes is only a few grid boxes. If the effective resolution is 10 grid boxes, then the smallest fully resolved spatial scales are 1000 km - the synoptic scale. If it is a goal to represent, for example, summer time lake-induced circulations, which are important weather and climate features, then the model must be able to resolve flows on the order of $1 - 10$ km. If this is the resolved scale, then the grid size needs to be order $0.1 - 1.0$ km. This suggests a type of model-structure uncertainty that requires interpretation and description when considering, for example, regional climate change.

The analysis performed in this paper can be used to assess numerical schemes. This analysis can only be applied to linear schemes, and does not inform us directly about non-linear schemes such as those with flux-limiters. However, we have already modified the methodology to two-dimensional non-linear numerical schemes, and this will appear in a future paper. It also provides robust guidance optimizing the choice of spatial resolution. This influences the decisions about computational design and resource management. With regards to timestep decisions an analysis with this method reveals the behavior of schemes with respect to Courant number, which is found to be large for higher order schemes. The inevitable gap between the grid-scale and effective resolution also provides am important insight into the description of uncertainty that is associated with variable grids, land-water

boundaries, steep topography and grid-scale physics.

Appendix A - Dispersion Analysis

The methodology for calculating the amplitude factor and dispersion relation of a given numerical scheme is as follows. We start by inserting the solution for the discrete tracer (8) into the scheme's discretization. The tracer mixing ratio at spatial index $j+\alpha$ and temporal index $n+\beta$, where $\alpha, \beta \in \mathbb{Z}$, is given as

$$q_{j+\alpha}^{n+\beta} = \hat{q}\exp(i(kx_{j+\alpha} - \omega t_{n+\beta})). \tag{.1}$$

We can now divide each term in the discretization by (8), to give a relationship between ω and k that depends on Δt and Δx. For any α and β, that term in the discretization becomes

$$\begin{aligned}\frac{q_{j+\alpha}^{n+\beta}}{q_j^n} =& \frac{\hat{q}\exp(i(kx_{j+\alpha} - \omega t_{n+\beta}))}{\hat{q}\exp(i(kx_j - \omega t_n))},\\ =& \exp(i(k\alpha\Delta x - \omega\beta\Delta t)).\end{aligned} \tag{.2}$$

To calculate the amplitude factor we separate (8) into temporal and spatial parts,

$$q_j^n = \hat{q}\exp\left(-i\omega t_n\right)\exp\left(ikx_j\right), \tag{.3}$$

and consider $\Gamma_{num} = \exp\left(-i\omega\Delta t\right)$. We substitute this into the scheme's discretization. From (.2) it follows that

$$\begin{aligned}\frac{q_{j+\alpha}^{n+\beta}}{q_j^n} =& \exp\left(-i\omega\beta\Delta t\right)\exp\left(ik\alpha\Delta x\right),\\ =& \left(\exp\left(-i\omega\Delta t\right)\right)^{\beta}\exp\left(ik\alpha\Delta x\right),\\ =& \Gamma_{num}^{\beta}\exp\left(ik\alpha\Delta x\right).\end{aligned} \tag{.4}$$

The resulting expression for the scheme's discretization can contain the amplitude factor to different powers. A two-time level scheme will only contain the amplitude factor to the power one, a three time-level scheme we obtain an expression which is quadratic in Γ, and a four time-level scheme gives a cubic equation for Γ. For powers greater than one, and hence the solution of quadratic or cubic equations, the correct root must be selected to give the actual amplitude factor of the physical mode, and not that of the computational mode.

Appendix B - Effective Resolution Threshold

The choice of the threshold ϵ will have a large impact on which wavenumbers are classified as resolved. This is demonstrated in Figure .9, where the effective resolution is calculated

for the third-order Lax-Wendroff scheme for a variety of Courant numbers, $0 < c \leq 1$. The effective resolution when only the diffusive component is considered is shown in the left plot, the effective resolution when only the dispersive component is considered is shown in the center plot, and the effective resolution when both the diffusive and dispersive components are considered is shown in the right plot. Different values of the threshold ϵ are shown: 0.005, 0.01, 0.05, 0.1 and 0.25. These correspond to the numerical amplitude factor and dispersion relation being within 99.5%, 99%, 95%, 90% and 75% respectively of the true value. For too stringent a threshold, $\epsilon = 0.005$, almost any deviation from the exact solution will result in that wavenumber being classed as unresolved. For too lenient a threshold, $\epsilon = 0.25$, large diffusion and dispersion errors will still be admissible in a resolved wave. Following [44] we choose $\epsilon = 0.01$, i.e. the numerical dispersion relation and amplitude factor must be within 99% of the analytic value.

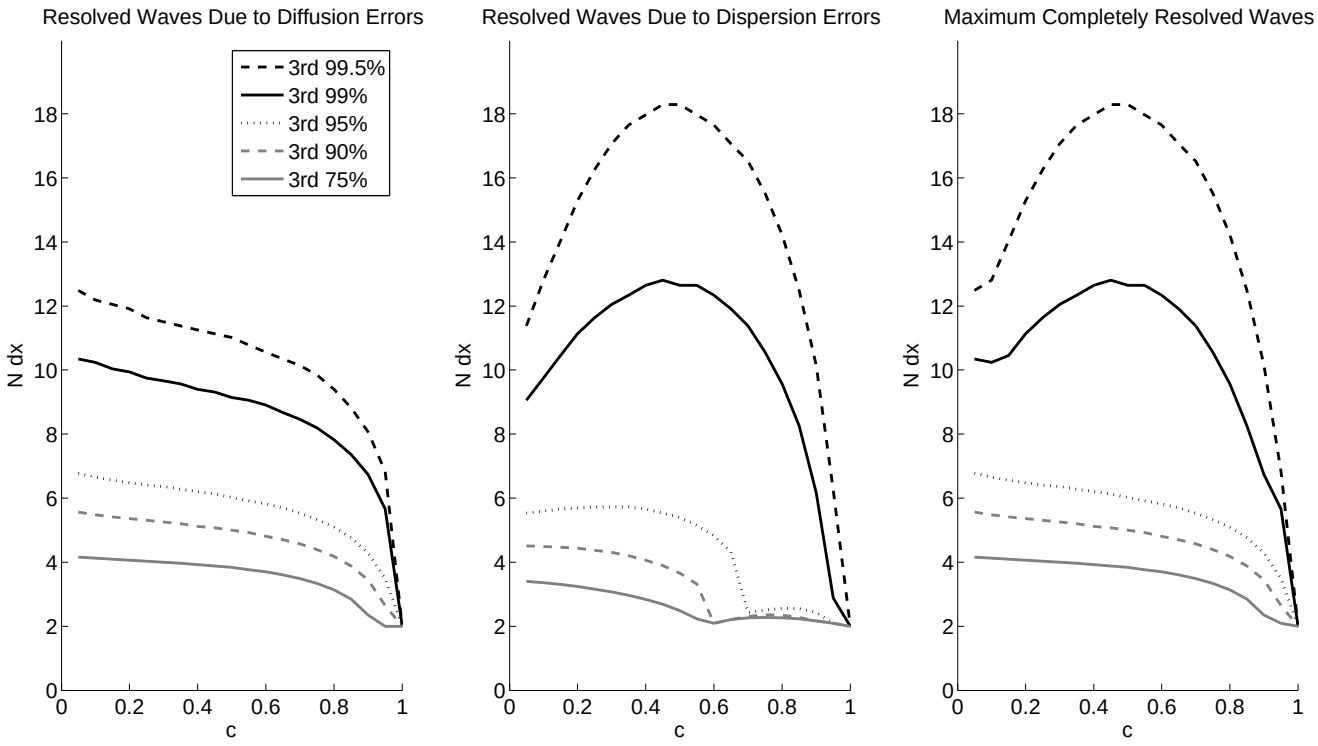

Figure .9: The effects of the choice of threshold ϵ on effective resolution for a third-order Lax-Wendroff type scheme for different Courant numbers c. The left plot shows the maximum resolved wave (in terms of $N\Delta x$) due to diffusion errors, the center plot shows the maximum resolved wave due to dispersion errors, and the right plot shows the maximum resolved wave due to both diffusion and dispersion errors.

Acknowledgements

The work was supported by the Office of Science, U.S. Department of Energy, Award No. DE-SC0006684.

References

[1] Aluie, H. and Kurien, S. 2011. Joint downscale fluxes of energy and potential enstrophy in rotating stratified Boussinesq flows. *EPL*, **96**, 44006.

[2] Asselin, R. 1972. Frequency filter for time integrations. *Monthly Weather Review*, **100**, 487-490.

[3] Bala, G., Rood, R. B., Bader, D., Mirin, A., Ivanova, D. and Drui, C. 2008. Simulated climate near steep topography: Sensitivity to numerical methods for atmospheric transport. *Geophys. Res. Lett.*, **35**, L14807.

[4] Colella, P. and Woodward, P. R. 1984. The Piecewise Parabolic Method (PPM) for gas-dynamical simulations. *J. Comput. Phys.*, **54**, 174-201.

[5] Charney, J. G., Fjortoft, R. and von Neumann, J. 1950. Numerical integration of the barotropic vorticity equation. *Tellus*, **2**, 237-254.

[6] Davies, T., Cullen, M. J. P., Malcom, A. J., Mawson, M. H., Staniforth, A., White, A. A. and Wood, N. 2005. A new dynamical core for the Met Office's global and regional modelling of the atmosphere. *Quart. J. Roy. Meteor. Soc.*, **131**, 1759-1782.

[7] Dennis, J. M., Edwards, J., Evans, K. J., Guba, O., Lauritzen, P. H., Mirin, A. A., St-Cyr, A., Taylor, M. A. and Worley, P. H. 2012. CAM-SE: A scalable spectral element dynamical core for the Community Atmosphere Model *Int. J. High Perf. Comput. Appl.*, **26**, 74-89.

[8] Dubal, M., Staniforth, A. and Wood, N. 2006. Some numerical properties of approaches to physics-dynamics coupling for NWP. *Quart. J. Roy. Meteor. Soc.*, **132**, 27-42.

[9] Durran, D. R. 1991. The Third-Order Adams-Bashforth Method: An Attractive Alternative to Leapfrog Time Differencing. *Monthly Weather Review*, **119**, 702-720.

[10] Fox-Rabinovitz, M. S., Stenchikov, G. L., Suarez, M. J and Takacs, L. L. 1997. A Finite-Difference GCM Dynamical Core with a Variable-Resolution Stretched Grid. *Mon. Weather Rev.*, **125**, 2943-2968.

[11] Fraedrich, K., Kirk, E., Luksch, U. and Lunkeit, F. 2005. The Portable University Model of the Atmosphere (PUMA): Storm track dynamics and low frequency variability. *Meteorol. Zeitschrift,*, **14**, 735-745.

[12] Fraedrich, K. 2012. A suite of user-friendly global climate models: Hysteresis experiments. *Eur. Phys. J. Plus,*, **127**, 53. DOI 10.1140/epjp/i2012-12053-7

[13] Gottlieb, S., Ketcheson, D. I. and Shu, C.-W. 2011. Strong Stability Preserving Runge-Kutta and Multistep Time Discretizations. *World Scientific Publishing, New Jersey (USA)*

[14] Hirt, C. W. 1968. Heuristic Stability Theory for Finite-Difference Equations. *J. Comput. Phys.*, **2**, 339-355.

[15] Hu, F. Q., Hussaini, M. Y. and Rasetarinera, P. 1999. An Analysis of the Discontinuous Galerkin Method for Wave Propagation Problems. *J. Comput. Phys.*, **151**, 921-946.

[16] Hundsdorfer, W. B., Koren, B., van Loon M. and Verwer, J. G. 1995. A positive finite-difference advection scheme. *J. Comput. Phys.*, **117**, 35-46.

[17] Jablonowski, C. and Williamson, D. L. 2011. The pros and cons of diffusion, filters and fixers in atmospheric general circulation models, in: Lauritzen, P. H., Jablonowski, C., Taylor, M. A. and Nair, R. D. (Eds), Numerical Techniques for Global Atmospheric Models, *Springer*, pp. 381-493.

[18] Kent, J., Thuburn, J. and Wood, N. 2012. Assessing Implicit Large Eddy Simulation for Two-Dimensional Flow. *Q. J. R. Met. Soc.*, **138**, 365-375.

[19] Kent, J., Jablonowski, C., Whitehead, J. P. and Rood, R. B. 2012. Downscale cascades in tracer transport test cases: an intercomparison of the dynamical cores in the Community Atmosphere Model CAM5. *Geo. Model Dev.*, **5**, 1517-1530.

[20] Kreiss, H.-O. and Oliger, J. 1972. Comparison of accurate methods for the integration of hyperbolic equations. *Tellus*, **24**, 199-215.

[21] Lander, J. and Hoskins, B. 1997. Believable Scales and Parameterizations in a Spectral Transform Model. *Mon. Weather Rev.*, **125**, 292-303.

[22] Lauritzen, P. H. 2009. A Stability Analysis of Finite-Volume Advection Schemes Permitting Long Time Steps. *Mon. Weather Rev.*, **135**, 2658-2673.

[23] Lauritzen, P. H., Nair, R. D. and Ullrich, P. A. 2010. A Conservative Semi-Lagrangian Multi-tracer transport scheme (CSLAM) on the cubed-sphere grid. *J. Comput. Phys.*, **229**, 1401-1424.

[24] Lax, P. D. and Wendroff, B. 1960. Systems of conservation laws. *Commun. Pure Appl. Math.*, **13**, 217-237.

[25] Lin, S. J. 2004. A "vertically Lagrangian" finite-volume dynamical core for global models. *Mon. Weather Rev.*, **132**, 2293-2307.

[26] Lin, S. J. and Rood, R. B. 1996. Multidimensional Flux-Form Semi-Lagrangian Transport Schemes. *Mon. Weather Rev.*, **124**, 2046-2070.

[27] Long, D. and Thuburn, J. 2011. Numerical wave propagation on non-uniform one-dimensional staggered grids. *J. Comput. Phys.*, **230**, 2643-2659.

[28] Margolin, L. G. and Rider, W. J. 2002. A rationale for implicit turbulence modelling. *Int. J. Numer. Meth. Fluids*, **39**, 821-841.

[29] Mason, P. J. 1994. Large-eddy simulation: A critical review of the technique. *Q. J. R. Meteorol. Soc.*, **120**, 1-26.

[30] McDonald, A. 1984. Accuracy of Multiply-Upstream, Semi-Lagrangian Advective Schemes. *Mon. Weather Rev.*, **112**, 1267-1275.

[31] Melvin, T., Staniforth, A. and Thuburn, J. 2012 Dispersion analysis of the spectral element method. *Q. J. R. Meteorol. Soc.*, **138**, 1934-1947. DOI:10.1002/qj.1906

[32] Neale, R. B., Chen, C.-C., Gettelman, A., Lauritzen, P. H., Park, S., Williamson, D. L., Conley, A. J., Garcia, R., Kinnison, D., Lamarque, J.-F.,Marsh, D., Mills, M., Smith, A. K., Tilmes, S., Vitt, F., Cameron-Smith, P., Collins, W. D., Iacono, M. J., Rasch, P. J., Taylor, M. A. Description of the NCAR Community Atmosphere Model (CAM 5.0). 2010. *NCAR Tech. Note NCAR/TN-486+STR*, pp. 1-268.

[33] Randall, D. 1994. Geostrophic adjustment and the finite-difference shallow-water equations. *Mon. Weather Rev.*, **122**, 1371-1377.

[34] Robert, A. 1966. The Integration of a Low Order Spectral Form of the Primitive Meteorological Equations. *Journal of the Meteorological Society of Japan*, **44**, 237-245.

[35] Rood, R. B. 1987. Numerical advection algorithms and their role in atmospheric transport and chemistry models. *Reviews of Geophysics*, **25**, 71-100.

[36] Skamarock, W. C. 2004. Evaluating Mesoscale NWP Models Using Kinetic Energy Spectra. *Mon. Weather Rev.*, **132**, 3019-3032.

[37] Skamarock, W. C. 2008. A linear analysis of the NCAR CCSM finite-volume dynamical core. *Mon. Weather Rev.*, **136**, 2112-2119.

[38] Thuburn, J. 2008. Some Conservation Issues for the Dynamical Cores of NWP and Climate Models. *Journal of Computational Physics*, **227**, 3715-3730.

[39] Tremback, C. J., Powell, J., Cotton, W. R. and Pielke, R. A. 1987. The forward-in-time upstream advection scheme: extension to higher orders. *Mon. Weather Rev.*, **115**, 540-555.

[40] Ullrich, P. A. and Jablonowski, C. 2011a. An analysis of 1D finite-volume methods for geophysical problems on refined grids. *J. Comput. Phys.*, **230**, 706-725.

[41] Ullrich, P. A. and Jablonowski, C. 2011b. Operator-Split Runge-Kutta-Rosenbrock (RKR) Methods for Nonhydrostatic Atmospheric Models. *Mon. Weather Rev.*, **140**, 1257-1284.

[42] Ullrich, P. A. and Jablonowski, C. 2012. MCore: A nonhydrostatic atmospheric dynamical core utilizing high-order finite-volume methods. *J. Comp. Phys.*, **231**, 5078-5108

[43] Ullrich, P. A. and Norman, M. R. 2013. The Flux-Form Semi-Lagrangian Spectral Element (FF-SLSE) method for tracer transport. *Q. J. R. Meteorol. Soc.*, **in press**.

[44] Ullrich, P. A. 2013. Understanding the treatment of waves in high-order atmospheric models, Part I: The shortest resolved waves of the 1D linear wave equation. *Q. J. R. Meteorol. Soc.*, **in review**.

[45] Walters, M. K. 2000. Comments on "The Differentiation between Grid Spacing and Resolution and Their Application to Numerical Modeling". *Bull. American Meterol. Soc.*, **81**, 2475-2477.

[46] Whitehead, J. P., Jablonowski, C., Rood, R. B. and Lauritzen, P. H. 2011. A stability analysis of divergence damping on a latitude-longitude grid. *Mon. Weather Rev.*, **139**, 2976-2993.

[47] Wicker, L. J. and Skamarock, W. C. 2002. Time-Splitting Methods for Elastic Models Using Forward Time Schemes. *Mon. Weather Rev.*, **130**, 2088-2097.

[48] Williamson, D. L. 1999. Convergence of atmospheric simulations with increasing horizontal resolution and fixed forcing scales. *Tellus*, **51A**, 663-673.

[49] Williamson, D. L. 2007. The evolution of dynamical cores for global atmospheric models. *J. Meteor. Soc. Japan*, **85B**, 241-269.

[50] Williamson, D. L. 2008. Equivalent finite volume and Eulerian spectral transform horizontal resolutions established from aqua-planet simulations. *Tellus*, **60A**, 839-847.

[51] Williamson, D. L. and Olson, J. G. 1994. Climate Simulations with a Semi-Lagrangian Version of the NCAR Community Climate Model. *Mon. Weather Rev.*, **122**, 1594-1610.

[52] Zerroukat, M., Wood, N. and Staniforth, A. 2002. SLICE: A Semi-Lagrangian Inherently Conserving and Efficient scheme for transport problems. *Quart. J. Roy. Meteor. Soc.*, **128**, 2801-2820.